

Time-resolved spectroscopy of a homogeneous dielectric barrier discharge for soft ionization driven by square wave high voltage

Vlasta Horvatic¹ · Antje Michels² · Norman Ahlmann² · Günter Jestel² · Damir Veza³ ·
Cedomil Vadla¹ · Joachim Franzke²

Received: 8 July 2015 / Revised: 3 August 2015 / Accepted: 6 August 2015 / Published online: 22 August 2015
© Springer-Verlag Berlin Heidelberg 2015

Abstract Helium capillary dielectric barrier discharge driven by the square wave-shaped high voltage was investigated spatially and temporally by means of optical emission spectroscopy. The finding of the previous investigation conducted with the sinusoidal-like high voltage was confirmed, i.e., the plasma in the jet and the plasma in the capillary constitute two temporally separated events. The plasma in the jet occurs prior to the discharge in the capillary and exists only during the positive half period of the applied high voltage. The time delay of the capillary discharge with respect to the discharge in the jet depended on the high voltage, and it was between 2.4 and 8.4 μ s for the voltage amplitude change in the range from 1.96 to 2.31 kV, respectively. It was found that, compared to sinusoidal-like voltage, application of the square wave high voltage results with stronger (~6 times) He line emission in the jet, which makes the latter more favorable for efficient soft ionization. The use of the square wave high voltage enabled comparison of the currents (~1 mA) flowing in the capillary during the positive and negative high voltage periods, which yielded the estimation for the charge dissipated in the atmosphere ($(4 \pm 20\%) \times 10^{-11}$ C) through the plasma jet.

Keywords Dielectric barrier discharge ionization · Soft ionization · Time-resolved emission spectroscopy

Introduction

Dielectric barrier discharge ionization (DBDI) technique [1] gained the popularity as a method for soft ionization of molecules due to its simplicity and adaptability of operation to different environments. DBD has numerous applications in analytical chemistry because it can generate mild, stable discharge at atmospheric pressure and low temperatures, rich with a large amount of chemically active species. They are easy to set up in simple and compact way, have low power consumption, and can operate over a wide pressure range with different discharge gasses. Therefore, the DBDs have found a wide range of analytical applications, such as the DBD atomizer for analytical atomic spectrometry [2, 3], DBD detector for gas chromatography [4], DBD-induced and/or assisted chemiluminescence [5, 6], and as the ionization source for ion-mobility spectrometry [7]. A comprehensive presentation of the history, principles, development, applications, and future prospects of this ionization source can be found in several reviews and articles [8–13].

The key constituent of this technique, which acts as efficient ionization source, is the atmospheric pressure plasma jet generated by dielectric barrier discharge. The formation and the dynamics of the plasma jets in the capillary dielectric barrier discharges have been extensively studied [14–20]. These investigations have shown that the jet is formed of well-directed ionization fronts, so called “plasma bullets,” which travel with the velocities several orders of magnitude higher than the gas flow velocity. The widespread concept of the jet development, i.e., plasma bullet formation and propagation, is based on a streamer discharge model proposed by Lu and Laroussi [21], within which the jet is considered to be a flow driven effluent of the discharge in the capillary.

However, in two previous experiments [14, 19], it was observed that the formation of the jet was independent of the ignition of a dielectric barrier discharge inside the capillary, but

✉ Vlasta Horvatic
blecic@ifs.hr

¹ Institute of Physics, Bijenicka 46, 10000 Zagreb, Croatia

² ISAS—Leibniz Institut für analytische Wissenschaften, Bunsen-Kirchhoff-Str. 11, 44139 Dortmund, Germany

³ Department of Physics, Faculty of Science, University of Zagreb, Bijenicka 32, 10000 Zagreb, Croatia

this phenomenon was not studied in detail. Recently [22], an extensive investigation of the helium capillary dielectric barrier discharge sustained by a quasi-sinusoidal high voltage has been reported. The spectrally, spatially, and temporally resolved emission from the discharge was measured simultaneously with plasma current. It was found that two plasmas separated in time were formed. First, an early plasma, which protrudes in the surrounding atmosphere in the form of the plasma jet, was formed. Subsequently, the plasma between the electrodes, which coincides with the ignition of the discharge in the capillary, occurred. The plasma jet, which is an essential part of a capillary DBD applied for soft ionization, occurred with appreciable strength and length only during the rise of the high voltage and in the period of time before the electrode plasma was ignited. No plasma jet was formed during the negative period of the high voltage. Very weak and short plasma jet, not convenient for soft ionization purposes, was formed during the electrode plasma ignition.

The present investigation deals with the formation and development of the homogeneous helium capillary dielectric barrier discharge (DBD) driven by square wave high voltage. It is known that DBD can operate in either filamentary or homogeneous mode [23], and it was demonstrated that the latter is characterized by significantly larger ionization efficiency of organic molecules [24, 25].

Here, it will be shown that the square wave voltage shape is more appropriate for producing the homogeneous mode operation than the sinusoidal-like one. In addition, with the square wave high voltage (HV) applied, the DBD can run at much lower HV amplitudes than in the case of the sinusoidal-like one. The present investigation examines the influence of the shape and the amplitude of the applied HV on the properties of He capillary DBD. The operation of DBD was investigated by time and spatially resolved OES measurements of the helium 706 and 501 nm lines intensities, with square wave high voltage applied to the electrodes. The comparison with recent results [22] obtained by using sinusoidal-like HV generator to operate

the DBD is made. In both cases, the spatiotemporal behavior of the measured emission was found to be generally very similar. It is shown that the square wave HV is much more suitable for getting better insight in the process of formation of the plasma jet than sinusoidal-like HV. Also, the direct comparison of the application of the two voltage shapes with nearly equal amplitudes and under the same working conditions showed that the plasma jet is much more intense in the case of square wave-shaped voltage than in the case of sinusoidal-like one.

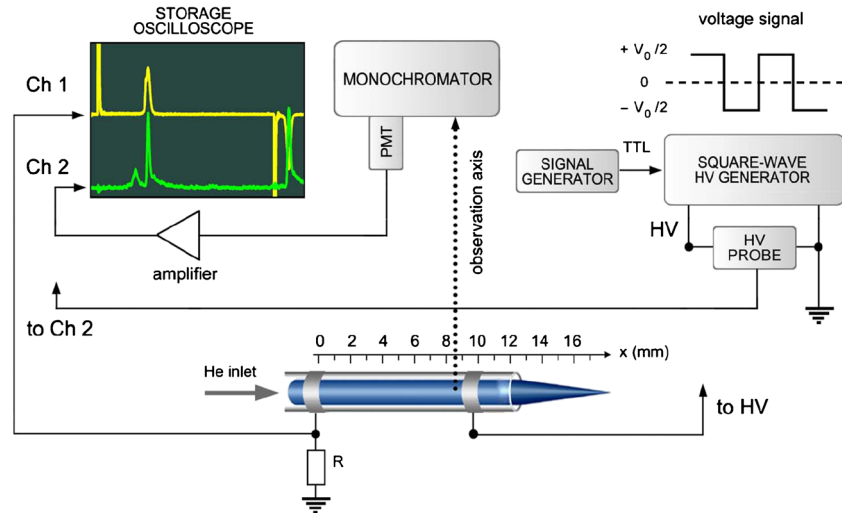
Experiment

The experimental setup is shown in Fig. 1. All the elements of the experimental arrangement, including one and the same capillary DBD, were the same as in the previous experiment [22], except the generator for supplying HV to the DBD electrodes. In order to get a reliable ionization source with no jumps from the homogeneous into the filamentary mode, a homemade generator was developed which produces square wave voltages with a rise time within 0.1 μ s and the peak-to-peak voltages up to 3.5 kV. With such generator, it was possible to sustain the DBD operation in a pure homogeneous mode over the whole applied HV amplitude range. Even when the geometry of the discharge was not perfect, the plasma would not switch to the filamentary mode. In a part of the present measurements, the generator delivering sinusoidal-like HV was used too.

The capillary glass tube outer and inner diameters were 1 and 0.5 mm, respectively. The working gas (He) flow was kept at the rate of 500 ml/min. The separation of the 1 mm wide electrodes was approximately 10 mm. The edge of the front (HV) electrode was at the distance of 2 mm from the capillary orifice. The rear electrode was connected to the ground by a resistor $R=100 \Omega$ which was used for the discharge current measurement.

OES measurements were performed mostly by monitoring the emission of the He 706 nm line, but in a part of this

Fig. 1 Experimental setup



experiment, the He 501 nm line intensity was measured too. The emission from the plasma source was collected at right angles with respect to the capillary axis x with a lens ($f=10$ cm) and imaged (1:1) onto the entrance slit of a 1-m McPherson monochromator (grating, 1200 grooves/mm). Both entrance and output slits were 0.3 mm wide, yielding the band pass of the monochromator of 0.3 nm. The monochromator was equipped with either EMI 9588QA (visible and near IR) or EMI 9789 (UV and visible) photomultiplier to measure He 706 nm and He 501 nm emission, respectively. The photomultiplier currents were converted to the voltage by a homemade amplifier (rise time, 0.8 ns), which was monitored by 70-MHz digital storage oscilloscope (Agilent DSO-X 2002A). The temporal behavior of the He emission was measured step-by-step at various positions along the x -axis by translating the DBD. The spatial resolution $dx=0.3$ mm was defined by the imaging ratio and the entrance slit width. In the first part of the experiment, the spatiotemporal behavior of the intensity of the He 706 nm line was measured for three square wave voltages ($V_0^a=2.31$ kV, $V_0^b=2.17$ kV and $V_0^c=1.96$ kV). In the second part, the emissions of the He 501 nm line produced with a square wave HV of $V_0=3.2$ kV and sinusoidal-like HV with the peak-to peak voltage of 3.8 kV were measured and compared.

Measurements and results

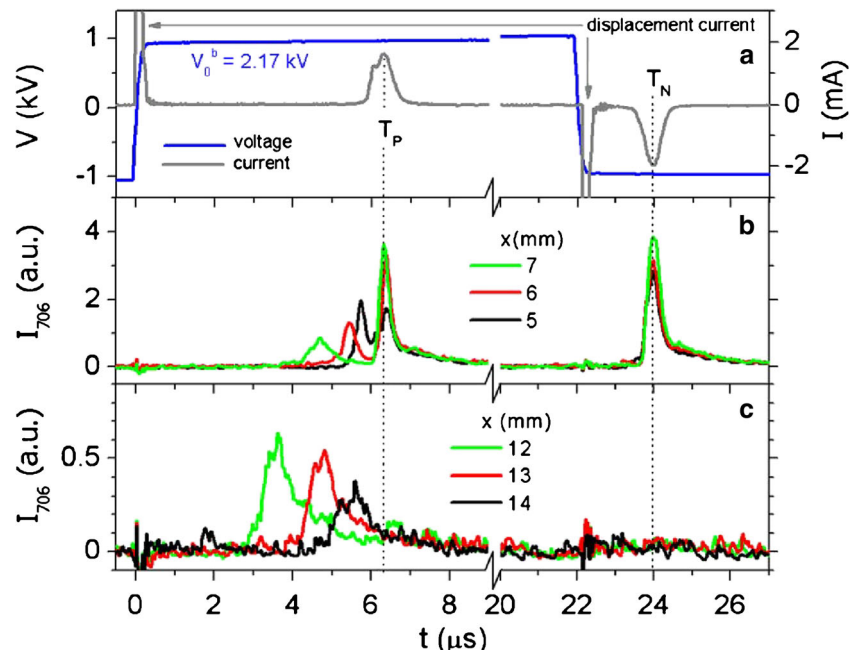
Measurements with the square wave high voltage

The time dependence of the applied square wave voltage with $V_0^b=2.17$ kV and the resulting current signals when the electrode plasma is ignited are shown in Fig. 2a.

Fig. 2 **a** Displacement currents and plasma currents recorded in the positive and negative square wave voltage period. **b** Time evolution of the emission intensities of the He 706 nm line measured at several axial positions inside the electrode plasma. **c** Time evolution of the He 706 nm line emission intensities at several axial positions along the plasma jet

The positive and negative voltage slopes coincide with the corresponding sharp charge displacement current peaks. The displacement current is proportional to the voltage derivative $dV(t)/dt$ and it is present only at the rising and falling voltage edge. The time scale origin ($t=0$) is set to coincide with the positive slope of the HV signal, i.e., with the rising slope of the corresponding displacement current. Note that the time scale is truncated from 9 to 20 μ s. The positive plasma current follows the positive displacement current after $T_P=6.2$ μ s, while the negative plasma current occurs at $T_N=1.9$ μ s with respect to the negative displacement current. The difference between the plasma occurrence times in the positive and negative voltage periods may be attributed to the influence of the charge accumulation on the capillary wall beneath the electrodes [26]. The dynamic electric field, resulting from the applied high voltage and wall charge, may differ in the positive and negative period, causing the plasma ignition at different times. Also, the part of the total energy in the positive voltage period is already consumed by the jet prior to occurrence of the capillary discharge. In the negative period, when the jet is not formed, the whole energy is at disposal for dissipation solely in the capillary plasma, enabling earlier ignition.

The time evolution of the emission intensities I_{706} of the He 706 nm line was measured in steps of 0.5 mm starting from the rear electrode ($x=0$), then along the capillary and up to the position $x=16$ mm in the plasma jet. The two-channel oscilloscope was triggered by the positive displacement current. The transient emission intensities measured at three x positions inside and three positions outside the capillary are shown in Fig. 2b, c. As in the case of a sinusoidal-like driving voltage [22], during the positive voltage period, two emission signals



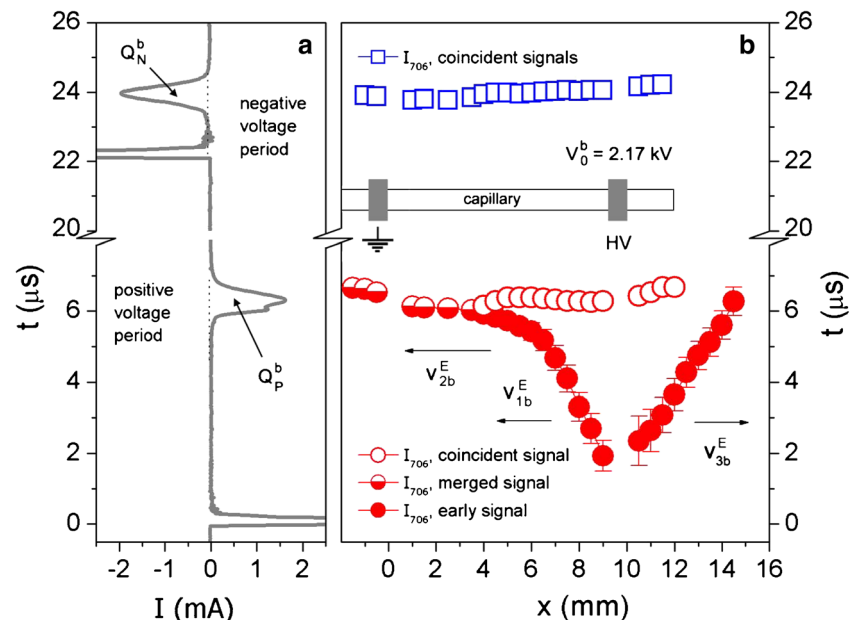
separated in time were observed. Their time separation depends on the point of observation x along the axis of the electrode plasma (see Fig. 2b). Emission signals, termed “coincident signals” in the following text, occur nearly at the ignition time T_B , i.e., coincide with the positive discharge current peak. The emission signals, which precede the coincident signals, i.e., positive plasma current, will be called “early signals.” As shown in Fig. 2c, in the plasma jet, only early signals appear during the positive voltage period. Nevertheless, very weak coincident signals can be observed in the region between the HV electrode and the capillary orifice when the positive voltage is applied. On the other hand, during the negative voltage period, only the signals, which coincide with the negative plasma current at ignition time T_N , were observed in the capillary. During this voltage period, there are no measurable emission intensities in the jet for $x > 10$ mm.

The spatiotemporal behavior of the He 706 nm line emission measured for $V_0^b = 2.17$ KV is presented in Fig. 3. In the picture, the position-dependent times at which the emission line intensity maxima occur (henceforth referred to as times of occurrence or occurrence times) are correlated with the plasma current signals in the same manner as in previous paper [22]. In both left and right part of Fig. 3, the time scales are on the ordinates. The current signal data for $V_0^b = 2.17$ kV are taken from Fig. 2a and re-plotted in Fig. 3a in the form of time vs. current diagram. Here, two important facts should be stressed. First, when looking at the shapes of the positive and negative plasma current peaks, it is apparent that the positive current peak is broader and exhibits a shoulder, which precedes the current maximum. Second, the integrals of the current signals over time represent the values of charges Q , which were transported through the resistor R (see Fig. 1) and correspond to the plasma current in the capillary between the electrodes.

Fig. 3 Correlation between the plasma current and the spatiotemporal behavior of the He 706 nm line emission for the square wave driving voltage with the peak-to-peak value $V_0^b = 2.17$ kV. **a** Time vs. current diagram. The areas under the plasma current signals correspond to the charges Q_P^b and Q_N^b , which are transported through the resistor R (see Fig. 1) during the positive and negative voltage period, respectively. **b** The occurrence times of the emission signals as a function of axial position x . The arrows symbolize the direction of the propagation of the excitation of He atoms. See further explanations in text

The evaluated values Q_P^b and Q_N^b for the positive and negative voltage periods, respectively, amount to 1.01×10^{-9} C and 1.06×10^{-9} C. Their difference is relatively small (5 %) but definitely larger than the error bar of statistical uncertainty (2 %).

The position-dependent occurrence times for early and coincidence emission signals in dependence on the position x along the capillary and the jet are plotted in Fig. 3b. The initial early emission peak signals appear in the vicinity of the HV electrode about 4 μ s before the positive plasma current peak in the both $+x$ and $-x$ directions. The reciprocal slopes of the data in Fig. 3b yield the velocities v^E (termed excitation velocities in the following), which are attributed to the propagation of the excitation of the helium atoms. These velocities should not be confused with either the velocity of the excited atoms or the velocity of the electrons. For instance, the actual gas flow velocity is 10 m/s, which is several orders of magnitude smaller than all excitation velocities v^E evaluated here for the early signals. On the other hand, the velocities of electrons, which are capable to excite He atoms, are several orders of magnitude larger than v^E . The excitation velocities of early signals (full red circles in Fig. 3b) increase with the distance from the HV electrode. Inside the capillary, in the region between $x=9$ and $x=6$ mm, the v_{1b}^E for early signals amounts to about 0.7 km/s, while the mean value of v_{2b}^E from $x=6$ mm to $x=4$ mm is approximately 20 km/s. The excitation velocity for the coincident signals during the positive voltage period (open red circles in Fig. 3b) is obviously much higher but cannot be evaluated because the corresponding occurrence times are constant within the error bars. The same is valid for the region $x < 4$ where the early and the coincident peaks merge together (half filled red circles) as well as for coincident signals during the negative voltage period (open blue squares). The



occurrence times of the merged signals seem to be in correlation with the shoulder appearing before the maximum of the plasma current signal. In the whole region from the HV electrode to the end of the capillary ($x=12$) and along the whole plasma jet, the medium velocity v_{3b}^E of the early peak emission signal amounts to 1 km/s.

In order to study the influence of the applied voltage on the spatiotemporal behavior of the helium line emission, the measurements were performed for two additional square-shaped voltages ($V_0^c=2.31$ kV and $V_0^a=1.96$ kV).

For each applied voltage, there are two sets of data at disposal: signal occurrence times and signal peak intensities as functions of x position. The obtained results for occurrence times vs. x position are shown in Fig. 4 for positive voltages together with the data for $V_0^b=2.17$ kV previously plotted in Fig. 3. The corresponding spatial distributions of the He 706 nm line peak intensities as functions of x position for all three applied voltages are depicted in Fig. 5. In both Figs. 4 and 5, the data are presented for positive voltages only, i.e., in cases when the plasma jet is produced.

As shown in Fig. 4a, the ignition times T_P and the plasma current peaks for the positive voltages strongly depend on the voltage amplitudes. Also, the excitation velocities for the early signals in the vicinity of the HV electrode strongly rise with the increasing voltage. For instance, the evaluated values v_a^E and v_c^E are 2.63 and 0.57 km/s. On the other hand, the corresponding charges Q_P transferred through the capillary and the resistor R to the ground vary slowly and seem to be linearly dependent on the voltage amplitudes ($Q_P^a=1.14 \times 10^{-9}$ C, $Q_P^c=0.92 \times 10^{-9}$ C). As for the negative plasma currents (not shown here), the variation of the ignition time T_N with the applied voltage is relatively small ($T_N^a=1.55$ μ s, $T_N^c=2.05$ μ s) and the corresponding charges vary from $Q_N^a=$

Fig. 4 Correlation between the plasma current and the spatiotemporal behavior of the He 706 nm line intensities for positive periods of three square wave voltages. **a** Time vs. relevant plasma current signals. The areas under plasma current signals correspond to the charges Q_P^a , Q_P^b , and Q_P^c flowing through the capillary between the electrodes during the positive period of the corresponding applied voltages. **b** Occurrence times for emission signals as a function of the axial DBD position x . The arrows symbolize the direction of the propagation of the excitation of He atoms. See further explanations in text

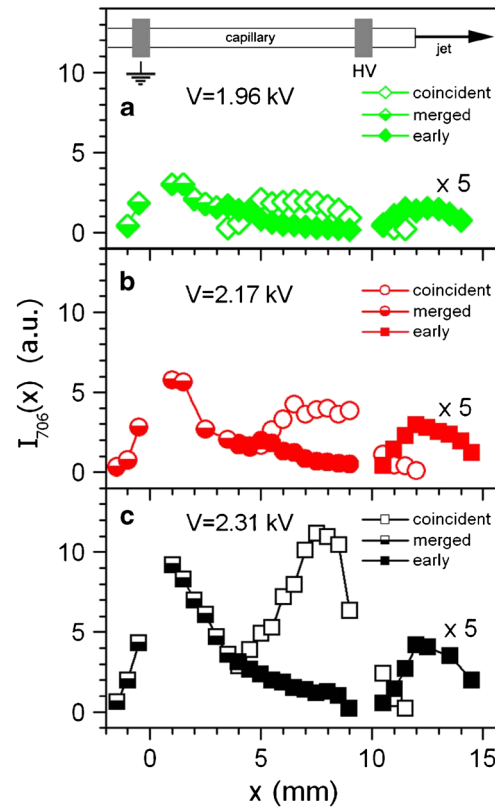
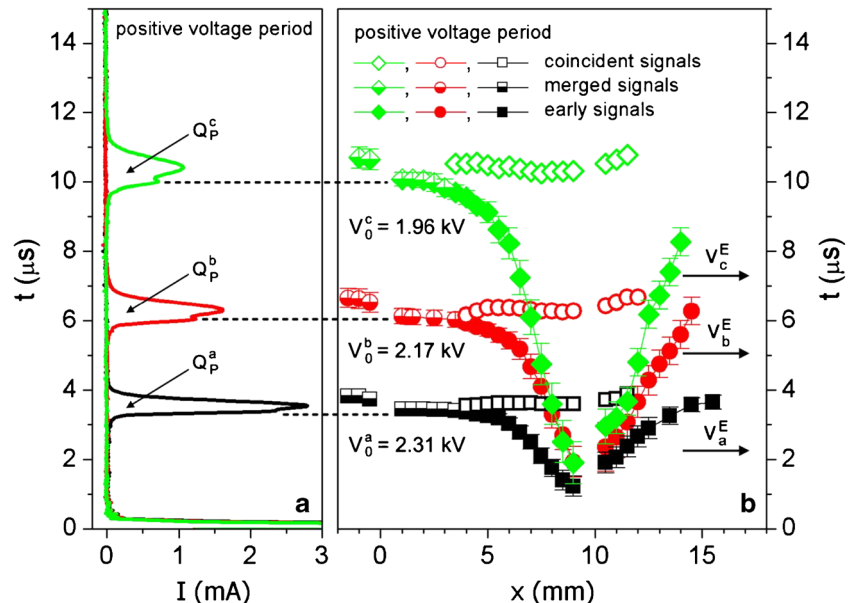


Fig. 5 **a–c** The peak emission intensities (in arbitrary units) of the He 706 nm line as a function of axial DBD position x for three applied voltages. The data for $x>10$ mm are magnified by a factor of 5

1.17×10^{-9} C to $Q_N^c=0.96 \times 10^{-9}$ C. The charge difference $\Delta Q=Q_N-Q_P$ in the applied voltage range is nearly constant and amounts to $(4 \pm 20\%) \times 10^{-11}$ C.

As can be seen in Fig. 5, the spatial distributions of He 706 nm line peak emission intensities, both in the capillary



and in the jet, exhibit similar shape for all three investigated voltages. The intensities increase roughly proportional to plasma current peak values. This may be considered plausible for coincident signals, but not for early signals which occur prior to discharge ignition in the capillary. This issue will be addressed in the next section.

Comparison of the results obtained with the square wave and sinusoidal-like high voltage

In the second part of the experiment, the discharge current and emission signals for the He 501 nm line obtained with the square wave and sinusoidal-like high voltages of comparable amplitudes were examined, under otherwise the same experimental conditions (the same DBD geometry and He flow, 500 ml/min).

Here, it should be emphasized that the lowest value of the sinusoidal-like HV for which the DBD could be sustained was 3.8 kV. In order to realize comparable amplitudes of the two HV shapes, the chosen square wave driving voltage had to be somewhat higher than in the measurements presented in Figs. 4 and 5.

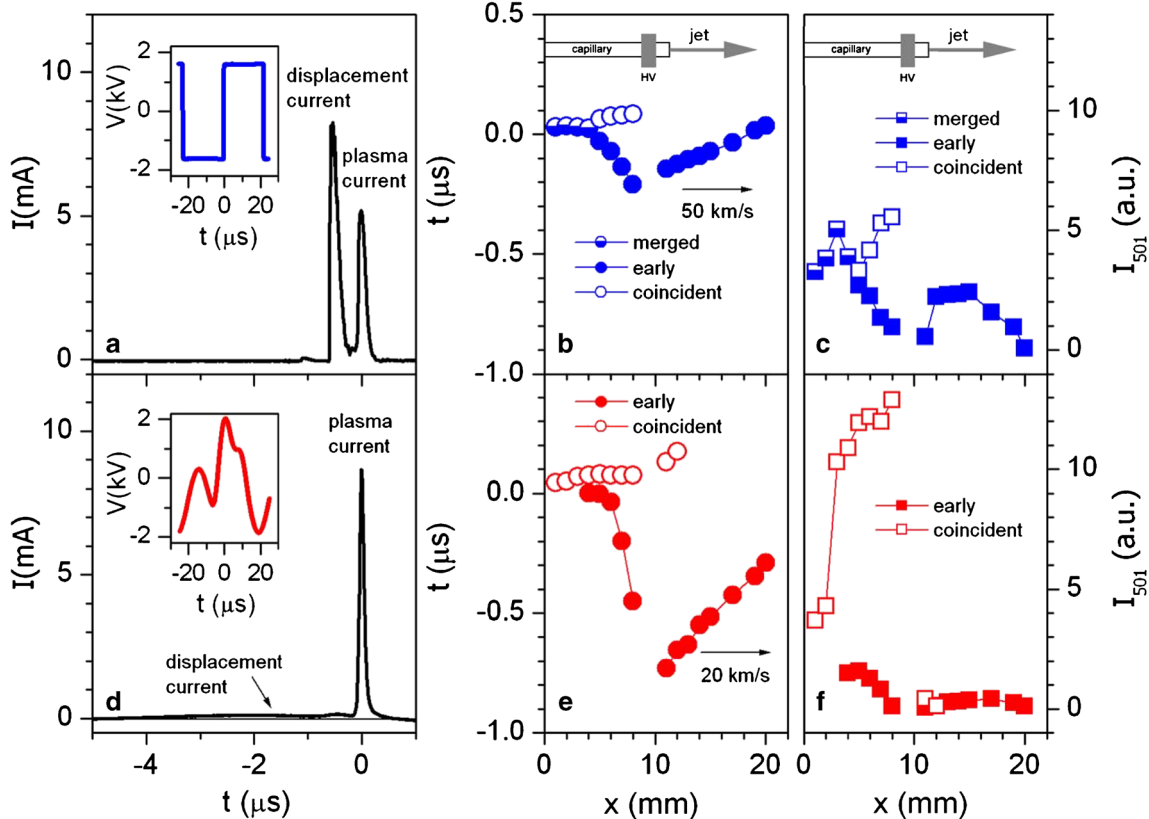


Fig. 6 Comparison of the DBD plasma currents and the spatiotemporal distributions of the He 501 nm line intensities measured under the same experimental conditions when the high voltages of different shapes are applied. The data are related to positive voltage periods only. **a, d** Charge displacement currents and plasma currents. *Insets* respective HV shapes.

The V_0 in the case of the square wave generator was 3.2 kV, while its value for the sinusoidal-like one was 3.8 kV. The measured currents, position-dependent occurrence times of merged, early and coincident signals, and spatial distributions of relative peak intensities of the He 501 nm line are presented in Fig. 6.

In the case of the square wave HV, the total charge Q_p^{SW} defined by the shape of the plasma current was 9.1×10^{-10} C, and for the negative voltage period (not shown here), the Q_n^{SW} is about 10 % larger than Q_p^{SW} . For the sinusoidal-like voltage, the peak current value is higher than in the former case but the evaluated Q_p^{SL} nearly equals to Q_p^{SW} . Different to the case of square wave voltage, the charge Q_n^{SL} in the negative sinusoidal-like period is about 30 % smaller than Q_p^{SL} in its positive period. However, it has to be mentioned that, as opposed to the square wave HV case, the ignition of the plasma in the positive and negative periods of the sinusoidal-like HV does not occur at the same absolute voltage values. These voltages are usually significantly different and in the present case amount to +1.9 and -1.2 kV.

The most important difference between the results obtained with two different voltage shapes is that the use of the square wave voltage yields more efficient excitation of He atoms in the

jet, which is clearly demonstrated by the corresponding peak intensities of the He 501 nm line depicted in Fig. 6c and f.

Discussion

In He DBDs with the configuration as in the present experiment, the jet constitutes an essential part of the DBD in the application for soft ionization. Namely, the spatial distribution of N_2^+ ions, which act as a precursor for the formation of the protonated water molecules essential for the soft ionization, exhibits a maximum in the plasma jet [23, 27], a few millimeters from the capillary orifice.

In general, the present time- and spatially resolved He line emission measurements confirm our findings in recently published work [22]. The plasma jet occurs only during the positive HV period and precedes the plasma ignition between the electrodes in the capillary. In the same manner as observed with sinusoidal-like HV, after the onset of the positive voltage, the propagation of He atoms excitation starts in the vicinity of the front HV electrode. Excited helium atoms are produced in collision with fast electrons, which are attracted by the positively charged HV electrode, and therefrom, the bulk excitation travels in both positive and negative x direction. During the positive voltage period, excited helium atoms first appear in the vicinity of HV electrode (see Figs. 3 and 4), meaning that at the very start of the process, free electrons become energetic enough to excite He atoms only after being accelerated all the way up to the HV electrode. At later times, the electrons gain enough energy to excite He atoms at distances further away from the HV electrode. This suggests that an overall electric field they experience is enhanced. The enhancement of the field could be due to the presence of the ionized nitrogen molecules N_2^+ . Namely, the relaxation of helium atoms in higher excited states eventually leads to accumulation of the population in the metastable states. In ambient atmosphere rich with nitrogen, Penning ionization of N_2 in collisions with He metastables takes place, resulting with creation of N_2^+ . Because nitrogen is always present as an impurity in the helium gas, the mentioned process is present in the capillary as well. Influenced by the electric field, N_2^+ molecules will move away from the HV electrode, and it is likely that a cloud of a positive space charge will be formed in front and behind the electrode, creating a transient effective electric field, which will accelerate electrons further.

Early emission of the He^* atoms was absent in the plasma jet region during the negative voltage period. In the case of negative polarity of the HV electrode, the free electrons will be accelerated away from it and will gain enough energy to produce He^* atoms at distances farther in the jet where the number density of He is substantially reduced. In the present experimental conditions, this would result with weak or non-measurable 706 nm radiation. The accompanying N_2^+ ions

will be attracted to the HV electrode and the formed cloud of a positive space charge will weaken the transient effective electric field. In turn, due to reduced acceleration, the electrons will become less capable of exciting He atoms, and the whole process will eventually cease, thus preventing the formation of the plasma jet.

When well-defined square wave HV is applied, it becomes apparent that charge Q_P transported through the capillary during the positive period is smaller than the charge Q_N in the negative period. The charges Q_P and Q_N for the square wave voltages applied here are of the order of magnitude 1×10^{-9} C and their differences $\Delta Q = Q_N - Q_P$ are always positive for the present electrode configuration. These differences can be attributed to the currents related to the plasma jet. The existence of the electrical current in the jet was qualitatively confirmed in our laboratory using an inductive current probe. It was found that the early signals in the jet coincide or are even delayed with respect to the jet current. However, the used current probe disturbs the plasma jet and no quantitative measurements could be performed. Technically speaking, the jet current occurs between HV electrode and an “ambient” ground. The assumed transport of ΔQ occurs along some effective path L_{eff} during the time ΔT between occurrence and cessation of the signal in the jet. The effective length can be estimated as the distance between the HV electrode edge and the end of the jet (in the present case: $L_{\text{eff}} \approx 5$ mm). This means that the ΔT can be defined as L_{eff}/v^E , which yields the simple expression $I_{\text{jet}} = v^E \Delta Q / L_{\text{eff}}$ for an approximate value of the plasma jet current. With the data given in the previous section, the calculated values of the plasma jet currents for the applied voltages 1.96, 2.17, and 2.31 kV were 4, 8, and 20 μA , respectively. It should be mentioned that within the error bars, the ratios of the relative He 501-nm line intensities in the jet (see Fig. 5) correspond to the ratios of the estimated I_{jet} values at various applied voltages. This is analogous to the relationship between the coincident peak intensities and the capillary plasma current, which was mentioned in the previous section.

Relatively small voltage increase of 15 % (from 1.96 to 2.31 KV) yielded five times larger plasma jet current. With increasing voltage, the excitation propagation velocities and consequently the plasma jet currents strongly increase. For instance, in the case presented in Fig. 6, related to the results obtained with the square wave HV with the amplitude of 3.2 kV, the excitation velocity was $v^E = 50$ km/s and the charge difference ΔQ amounted to $\approx 1 \times 10^{-10}$ C. With the effective length $L_{\text{eff}} \approx 5$ mm, this yielded $I_{\text{jet}} \approx 0.5$ mA. Our detailed ongoing experiments in a relatively wide voltage range verify the present consideration. The results of these experiments confirmed that the helium line intensities in the jet are linearly proportional with the evaluated jet currents.

Similar consideration can be made for the early signal propagation in the capillary during the positive voltage period

of a square wave HV. In contrast to the ΔQ , the excitation velocities in $-x$ direction indicate the existence of a part of the Q_p which contributes to the positive plasma current through the capillary before it reaches the maximum during the main capillary discharge. In this manner, the relatively broad and asymmetric positive current shapes with more or less pronounced early local maxima can be explained.

Conclusion

The presented spatiotemporal OES investigations of the He capillary DBD driven by the square wave-shaped high voltage confirm earlier [22] finding that the plasma in the jet and the capillary represent two events separated in time. The occurrence of the plasma in the jet precedes the discharge in the capillary and exists only during the positive period of the applied high voltage. It was shown that, compared to sinusoidal-like voltage, application of the square wave HV results with stronger He line emission in the jet. Because the properties of the jet are essential for the efficient soft ionization, this implies that the application of square wave HV is more gainful for that purpose. Also, the use of the square wave HV enabled comparison of the currents flowing in the capillary and the jet during the positive and negative HV periods, which yielded the estimation for the charge dissipated in the atmosphere through the plasma jet.

Acknowledgments The financial support by the Ministerium für Innovation, Wissenschaft und Forschung des Landes Nordrhein-Westfalen, the Bundesministerium für Bildung und Forschung, the Deutsche Forschungsgemeinschaft (project no. FR 1192/13-1) is gratefully acknowledged. This work has been supported in part by the Croatian Science Foundation under the project no. 2753.

Conflict of interest The authors declare that they have no conflict of interests.

References

- Na NM, Zhao X, Zhang SC, Yang CD, Zhang XR (2007) Development of a dielectric barrier discharge ion source for ambient mass spectrometry. *J Am Soc Mass Spectrom* 18(10):1859–1862
- Zhu Z, Liu J, Zhang S, Na X, Zhang X (2008) Determination of Se, Pb, and Sb by atomic fluorescence spectrometry using a new flameless, dielectric barrier discharge atomizer. *Spectrochim Acta B At Spectrosc* 63(3):431–436
- Yu Y, Du Z, Chen M, Wang J (2008) Atmospheric-pressure dielectric-barrier discharge as a radiation source for optical emission spectrometry. *Angew Chem Int Ed* 47(41):7909–7912
- Gras R, Luong J, Monagle M, Winniford B (2006) Gas chromatographic applications with the dielectric barrier discharge detector. *J Chromatogr Sci* 44(2):101–107
- He Y, Lv Y, Li Y, Tang H, Li L, Wu X, Hou X (2007) Dielectric barrier discharge-induced chemiluminescence: potential application as GC detector. *Anal Chem* 79(12):4674–4680
- Almasian MR, Na N, Wen F, Zhang S, Zhang X (2010) Development of a plasma-assisted cataluminescence system for benzene, toluene, ethylbenzene, and xylenes analysis. *Anal Chem* 82(9):3457–3459
- Jafari MT (2011) Low-temperature plasma ionization ion mobility spectrometry. *Anal Chem* 83(3):797–803
- Guo C, Tang F, Chen J, Wang X, Zhang S, Zhang X (2015) Development of dielectric-barrier-discharge ionization. *Anal Bioanal Chem* 407(9):2345–2364
- Hu J, Li W, Zheng C, Hou X (2011) Dielectric barrier discharge in analytical spectrometry. *Appl Spectrosc Rev* 46(5):368–387
- Meyer C, Müller S, Gurevich EL, Franzke J (2011) Dielectric barrier discharges in analytical chemistry. *Analyst* 136(12):2427–2440
- Bárdos L, Baránková H (2010) Cold atmospheric plasma: sources, processes, and applications. *Thin Solid Films* 518(23):6705–6713
- Tendero C, Tixier C, Tristant P, Desmaison J, Leprince P (2006) Atmospheric pressure plasmas: a review. *Spectrochim Acta B* 61(1):2–30
- Kogelschatz U (2003) Dielectric-barrier discharges: their history, discharge physics, and industrial applications. *Plasma Chem Plasma Process* 23(1):1–46
- Jiang N, Ji A, Cao Z (2009) Atmospheric pressure plasma jet: effect of electrode configuration, discharge behavior, and its formation mechanism. *J Appl Phys* 106(1):013308
- Urabe K, Morita T, Tachibana K, Ganguly BN (2010) Investigation of discharge mechanisms in helium plasma jet at atmospheric pressure by laser spectroscopic measurements. *J Phys D Appl Phys* 43(9):095201
- Sands BL, Leiweke RJ, Ganguly BN (2010) Spatiotemporally resolved Ar (1s₅) metastable measurements in a streamer-like He/Ar atmospheric pressure plasma jet. *J Phys D Appl Phys* 43(28):282001
- Boeuf J-P, Yang LL, Pitchford LC (2013) Dynamics of a guided streamer ('plasma bullet') in a helium jet in air at atmospheric pressure. *J Phys D Appl Phys* 46(1):015201
- Karakas E, Akman MA, Laroussi M (2012) The evolution of atmospheric-pressure low-temperature plasma jets: jet current measurements. *Plasma Sources Sci Technol* 21(3):034016
- Sands BL, Ganguly BN, Tachibana K (2008) A streamer-like atmospheric pressure plasma jet. *Appl Phys Lett* 92(15):151503
- Sands BL, Huang SK, Speltz JW, Niekamp MA, Ganguly BN (2013) Role of Penning ionization in the enhancement of streamer channel conductivity and Ar(1s5) production in a He-Ar plasma jet. *J Appl Phys* 113(15):153303
- Lu X, Laroussi M (2006) Dynamics of an atmospheric pressure plasma plume generated by submicrosecond voltage pulses. *J Appl Phys* 100(6):063302
- Horvatic V, Michels A, Ahlmann N, Jestel G, Veza D, Vadla C, Franzke J (2015) Time- and spatially resolved emission spectroscopy of the dielectric barrier discharge for soft ionization sustained by a quasi-sinusoidal high voltage. *J Anal Bioanal Chem*. doi:[10.1007/s00216-015-8827-7](https://doi.org/10.1007/s00216-015-8827-7)
- Müller S, Krähling T, Veza D, Horvatic V, Vadla C, Franzke J (2013) Operation modes of the helium dielectric barrier discharge for soft ionization. *Spectrochim Acta B* 85:104–111
- Meyer C, Müller S, Gilbert-López B, Franzke J (2013) Impact of homogeneous and filamentary discharge modes on the efficiency of dielectric barrier discharge ionization mass spectrometry. *Anal Bioanal Chem* 405(14):4729–4735
- Horvatic V, Vadla C, Franzke J (2014) Discussion of fundamental processes in dielectric barrier discharges used for soft ionization. *Spectrochim Acta B* 100:52–61

26. Urabe K, Ito Y, Osamu Sakai O, Tachibana K (2010) Interaction between dielectric barrier discharge and positive streamer in helium plasma jet at atmospheric pressure. *Jpn J Appl Phys* 49(10R): 106001
27. Chan GC-Y, Shelley JT, Wiley JS, Engelhard C, Jackson AU, Cooks RG, Hieftje GM (2011) Elucidation of reaction mechanisms responsible for afterglow and reagent-ion formation in the low-temperature plasma probe ambient ionization source. *Anal Chem* 83(10):3675–3686